Available online at www.sciencedirect.com

SCIENCE DIRECT®

Journal of Computational and Applied Mathematics 168 (2004) 53–63

JOURNAL OF COMPUTATIONAL AND APPLIED MATHEMATICS

www.elsevier.com/locate/cam

Numerical analysis of a single row of coolant jets injected into a heated crossflow

F. Bazdidi-Tehrani*, A. Shahmir, A. Haghparast-Kashani

College of Mechanical Engineering, Iran University of Science and Technology, Narmak, Tehran 16844, Iran

Received 20 September 2002; received in revised form 8 May 2003

Abstract

The objective of present work was to develop a three-dimensional numerical simulation on the basis of the finite volume method for predicting the penetration and mixing characteristics of a single row of coolant jets injected normally into a heated crossflow in a constant area duct. Two types of mesh size were developed to evaluate the ability of the standard and the (RNG)k–ε turbulence models. The effects of jet-to-mainstream momentum flux ratio, in the range of 6.0–23.5 and duct height to hole diameter ratio and relative spacing of adjacent jets to hole diameter ratio, within the range of 4.0–12.0 and 2.0–4.0, respectively, were investigated. Comparisons between the present numerical results on the temperature profiles and the experimental results of Holdeman and Walker (AIAA J. 15 (2) (1977) 243) demonstrated reasonable agreement.

Keywords: Finite volume; Coolant jets; Mixing; Temperature profiles

1. Introduction

The interaction of a subsonic circular jet with a subsonic deflecting stream has been the subject of interest in many engineering applications. This type of flow exhibits many features such as the production of large-scale eddies and high levels of turbulence, including flow reversal, which are of interest in basic fluid dynamics. The injection of air into the dilution zone of a gas turbine combustor, film cooling by normal injection of a coolant jet through discrete holes on a wall and smoke plumes from chimney stacks, are some notable examples. In the dilution zone of a gas turbine combustor, hot gas temperature profile at the outlet must be matched carefully to the turbine blade stress levels,

* Corresponding author. Tel.: +98-21-7491228X9; fax: +98-21-7454050.
E-mail address: bazdid@iust.ac.ir (F. Bazdidi-Tehrani).

0377-0427/$ - see front matter
doi:10.1016/j.cam.2003.05.012

if long turbine life is to be attained. So, it is usually desirable that the injected jet mixes fully and uniformly with the mainstream.

The objective of many studies has been to model the penetration and mixing characteristics of coolant air jets injected into a heated crossflow in a duct. Ramsey and Goldstein [16] carried out an experimental investigation on the mixing of a jet injected normally into a cross-stream. Cox [3] and Holdeman and Walker [11] developed an analytical model for predicting the temperature profile at the downstream of coolant jets, injected normally into a heated crossflow. Patankar et al. [15] did a numerical work for a jet injected normally into a crossing stream. They used the Finite Volume method and for modeling the turbulence, their choice was the standard k–ε model. Wittig et al. [19] worked on the temperature profile development in turbulent mixing of coolant jets with a hot crossflow. Holdeman et al. [8–10] worked on different experimental setups for developing the mixing characteristics at the dilution zone and, finally, investigated analytical formulas based on the geometrical and the flow variables, for predicting the exit temperature profile. Most of these studies were reviewed by Holdeman [5]. He showed that the rate of mixing and penetration of jets into the mainstream was mainly affected by two important factors: (a) geometrical variables and (b) flow variables. Holdeman et al. [7] developed a numerical method for the mixing of multiple coolant jets with a confined crossflow in a cylindrical duct. Holdeman et al. [6] summarized experimental and computational results on the mixing of opposed rows of jets with a confined subsonic crossflow in rectangular ducts. The studies from which these results were excerpted investigated flow and geometric variations typical of the complex three-dimensional flow field in the combustion chambers in gas turbine engines. Kroll et al. [12] investigated the characteristics that govern the optimal crossflow mixing in cylindrical ducts. Bazdidi-Tehrani and Haghparast [1] predicted the penetration of a single jet injected normally into an air crossflow with no temperature difference by means of Computational Fluid Dynamics. Bazdidi-Tehrani and Shahmir [2] developed a three-dimensional numerical simulation on the basis of the finite volume method for a nonreacting mixing process to predict the mixing characteristics of a single row of coolant jets injected normally into a heated crossflow.

The effect of independent flow and geometrical variables on the temperature profile and the penetration of coolant jets injected normally into a heated crossflow in a rectangular duct, have been studied in the present numerical work.

2. Governing equations

The time-averaged equations governing the motion of an incompressible, steady and constant property fluid, may be written in a reduced form, as follows [4]:

$$\frac{\partial U_i}{\partial x_i} = 0, \tag{1}$$

$$\rho U_j \frac{\partial U_i}{\partial x_j} = -\frac{\partial P}{\partial x_i} + \frac{\partial}{\partial x_j}\left(\mu \frac{\partial U_i}{\partial x_j} - \rho\overline{u_i' u_j'}\right), \tag{2}$$

$$U_i \frac{\partial T}{\partial x_i} = \frac{\partial}{\partial x_i}\left(\alpha \frac{\partial T}{\partial x_i} - \overline{u_i' T'}\right), \tag{3}$$

$$p = \rho R T, \tag{4}$$

where, $\rho, T, \alpha, U, x, p, \mu, R, u'$ and T' are density, time-averaged temperature, thermal diffusivity, time-averaged velocity, distance, static pressure, viscosity, gas constant, fluctuating velocity and temperature, respectively.

It is an unfortunate fact that no single turbulence model is universally accepted as being superior for all classes of problems. The choice of turbulence model will depend on considerations such as the physics encompassed in the flow, the established practice for a specific class of problem, the level of accuracy required, the available computational resources, and the amount of time available for the simulation.

The turbulent stresses, τ_{ij}, are related to the velocity gradients via a turbulent viscosity, μ_T. This relationship is called the Boussinesq approximation [18]:

$$\tau_{ij} = -\rho\overline{u_i' u_j'} = \mu_T \left(\frac{\partial U_i}{\partial x_j} + \frac{\partial U_j}{\partial x_i} \right) - \frac{2}{3} \rho k \delta_{ij}, \tag{5}$$

where, δ_{ij} is the Kronecker delta.

In the standard high Reynolds and renormalization group (RNG) k–ε models, the Eqs. (5) and (6) are used. In these equations, k is the turbulence kinetic energy and ε is the rate of dissipation [18]:

$$\mu_T = \rho C_\mu \frac{k^2}{\varepsilon}. \tag{6}$$

The simplest "complete models" of turbulence are two-equation models in which the solution of two separate transport equations allows the turbulent velocity and length scales to be independently determined. It is a semi-empirical model, and the derivation of the model equations relies on phenomenological considerations and empiricism. The standard high Reynolds k–ε model employs the following transport equations, which are used for obtaining k and ε [18]:

$$\rho U_j \frac{\partial k}{\partial x_j} = \tau_{ij} \frac{\partial U_i}{\partial x_j} - \rho\varepsilon + \frac{\partial}{\partial x_j} \left[\left(\mu + \frac{\mu_T}{\sigma_k} \right) \frac{\partial k}{\partial x_j} \right], \tag{7}$$

$$\rho U_j \frac{\partial \varepsilon}{\partial x_j} = C_{\varepsilon 1} \frac{\varepsilon}{k} \tau_{ij} \frac{\partial U_i}{\partial x_j} - C_{\varepsilon 2} \rho \frac{\varepsilon^2}{k} + \frac{\partial}{\partial x_j} \left[\left(\mu + \frac{\mu_T}{\sigma_\varepsilon} \right) \frac{\partial \varepsilon}{\partial x_j} \right], \tag{8}$$

where, the empirical constants are defined as follows [18]:

$$C_{\varepsilon 1} = 1.44,\ C_{\varepsilon 2} = 1.92,\ C_\mu = 0.09,\ \sigma_k = 1.0,\ \sigma_\varepsilon = 1.3. \tag{9}$$

The statistical mechanics approach has led to new mathematical formulation which, in conjunction with a limited number of assumptions regarding the statistics of small-scale turbulence, provides a rigorous basis for the extension of the Eddy viscosity model. The renormalization group (RNG) devised by Yakhot and Orszag (see Ref. [17]) has to date attracted most interest. This model represents the effects of the small-scale turbulence by means of a random forcing function in the Navier–Stokes equation. The RNG procedure systematically removes the small scales of motion from the governing equations by expressing their effects in terms of larger scale motions and a modified viscosity. The mathematics is highly abstruse. The (RNG) k–ε model employs the following transport

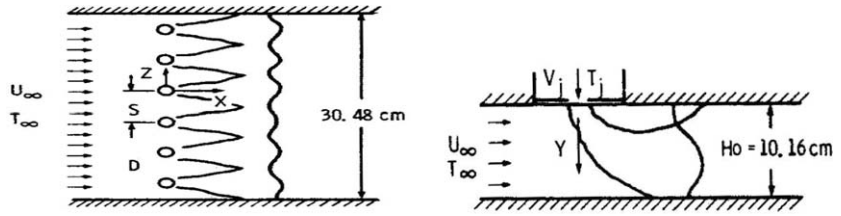

Fig. 1. Schematic of a single row of jets flow [11].

equations [17] (Fig. 1):

$$\rho U_j \frac{\partial k}{\partial x_j} = \frac{\partial}{\partial x_j}\left[(\alpha_k \mu_{\text{eff}})\frac{\partial k}{\partial x_j}\right] - \rho\overline{u_i' u_j'}\frac{\partial U_i}{\partial x_j} - \rho\varepsilon, \tag{10}$$

$$\rho U_j \frac{\partial \varepsilon}{\partial x_j} = \frac{\partial}{\partial x_j}\left[(\alpha_\varepsilon \mu_{\text{eff}})\frac{\partial \varepsilon}{\partial x_j}\right] - \frac{\varepsilon}{k} C_{1\varepsilon}^* \rho\overline{u_i' u_j'}\frac{\partial U_i}{\partial x_j} - C_{2\varepsilon}\rho\frac{\varepsilon^2}{k}, \tag{11}$$

$$\mu_{\text{eff}} = \mu + \mu_t, \tag{12}$$

$$C_{1\varepsilon}^* = C_{1\varepsilon} - \frac{\eta(1-\frac{\eta}{\eta_0})}{1+\beta\eta^3}, \tag{13}$$

$$\eta = \left(\tau_{ij}\frac{\partial U_i}{\partial x_j}\right)^{0.5}\frac{k}{\varepsilon}, \tag{14}$$

$$\beta = 0.012,\ \eta_0 = 4.377,\ C_{2\varepsilon} = 1.68,\ C_{1\varepsilon} = 1.42,\ \alpha_k = \alpha_\varepsilon = 1.39,\ C_\mu = 0.0845. \tag{15}$$

3. Flow geometry

The flow geometry (see Fig. 2) was selected according to the Holdeman and Walker's [11] experimental setup, as shown in Fig. 1.

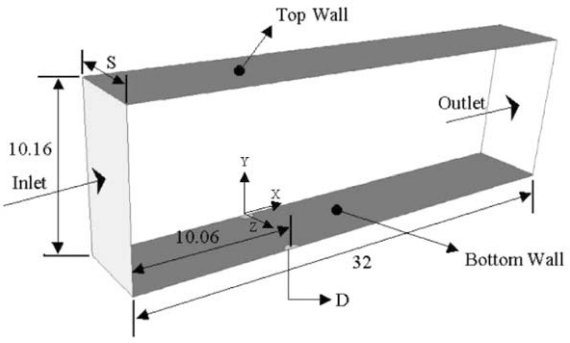

Fig. 2. The geometry of the computational domain (dimensions in cm).

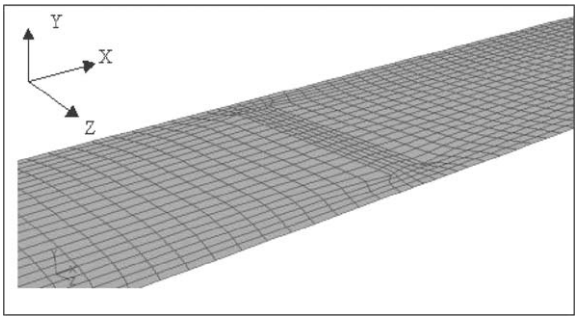

Fig. 3. The mesh including two adjacent holes at the bottom wall.

4. Grid generation

Computational fluid dynamics (CFD) methods, based on Cartesian or cylindrical coordinate systems, have certain limitations regarding irregular geometries [17], such as the geometry of a jet cross-section which is connected to a duct, as in the present work. Methods based on the body-fitted grid or the nonorthogonal grid systems, do not have such limitations and hence, in this paper, the body-fitted grid was used. Two structured mesh sizes were employed to verify the independence of present numerical solution from the mesh size. The fine and coarse grids were $(140 \times 35 \times 28)$ and $(71 \times 35 \times 18)$, respectively. Fig. 3 illustrates a typical mesh generated, including two adjacent jet holes at the bottom wall of the geometry shown in Fig. 2.

5. Numerical details

The present numerical solution employed the finite volume based finite difference method [14] and it included the following details:
(1) Solution of the governing equations on the basis of three-dimensional Cartesian coordinates, with adaptive grids and variable density was employed. (2) The power-law scheme was used to discretize the convection terms. (3) The SIMPLE algorithm was employed to correct the pressure term. (4) The standard k–ε and RNG k–ε models with wall functions were used. (5) The mixing was considered as a nonreacting flow. (6) The value of 0.0000001 (i.e., 1×10^{-7}) was considered for the convergence criterion of the energy equation and 0.0001 (i.e., 1×10^{-4}) for the other equations.

6. Boundary conditions

As shown in Fig. 2, the computational domain had eight boundaries where dependent variables were specified. An inlet and an outlet plane of the duct, two symmetry planes, two inlet planes for the jets, and two solid walls at the top and bottom. At the inlet boundaries, uniform profiles of velocity and temperature were specified from the experimental data [11]. Where, $T_\infty = 600$ K, $U_\infty = 15$ m/s, $T_j = 300$ K and $U_j = 24.3$–78.5 m/s were taken as the inlet conditions. The turbulent intensity of mainstream and jets were set as 1% and 3%, respectively [17]. At the outlet, sufficiently far from

the jets, a zero gradient was considered as the boundary condition for all the variables, except the pressure. The side walls were assumed as symmetry boundary conditions. On the symmetry plane (X–Y plane), the normal velocity vanished and the normal derivatives of the other variables were considered as zero. The top and bottom walls assumed as adiabatic and the wall function method was used [17]. The jet-to-mainstream momentum flux ratio was defined as: $J=(\rho_j U_j^2)/(\rho_\infty U_\infty^2)$, in the range of 6–23.4. For the present work, the hole discharge coefficient, C_d, varied from 0.66, at the lowest J, to 0.62, at the highest J [11]. The results for the temperature field were presented as vertical profiles of the dimensionless temperature difference ratio, $\theta=(T_\infty-T)/(T_\infty-T_j)$, where, T is the local temperature, T_∞ is the mainstream total temperature and T_j is the jet total temperature. The largest value of $\theta(\theta=1)$ corresponded to the coolest regions of the flow.

7. Results

Fig. 4 shows clearly that the fine grid ($140\times35\times28$) gave a much better agreement with the experimental results of Holdeman and Walker [11], in comparison with the coarse grid ($71\times35\times18$). Hence, the fine grid was employed throughout the present work.

Fig. 5 demonstrates comparisons between the present numerical results, based on two turbulence models, and the experimental results of Holdeman and Walker [11]. It can be seen that the (RNG)

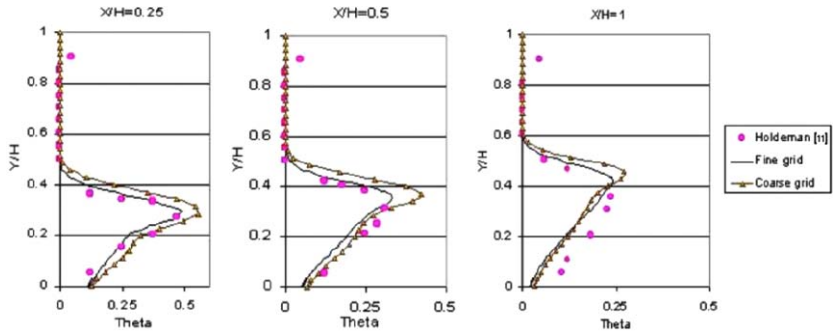

Fig. 4. Effect of mesh size on the temperature profiles, downstream of jets ($J=6$, $S/D=4$, $H/D=8$).

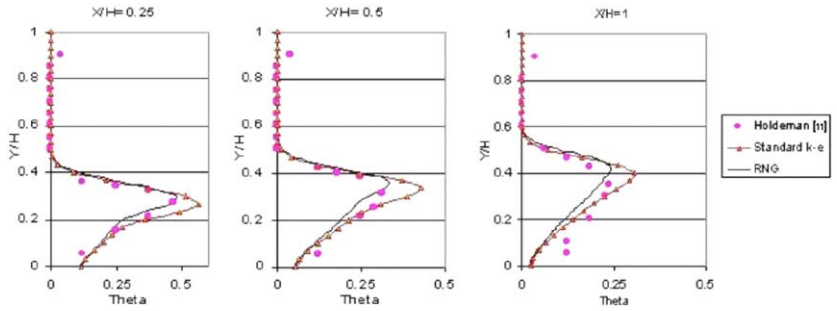

Fig. 5. Effects of turbulence models on the temperature profile downstream of jets ($J=6$, $S/D=4$, $H/D=8$).

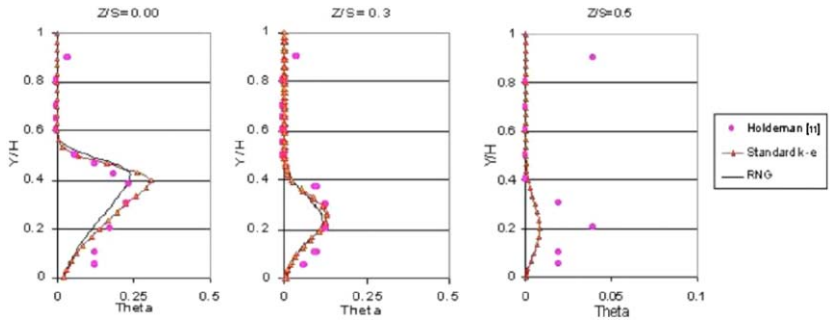

Fig. 6. Effects of turbulence models on the temperature profile with distance from center-plane ($J = 6$, $S/D = 4$, $H/D = 8$, $X/H = 1$).

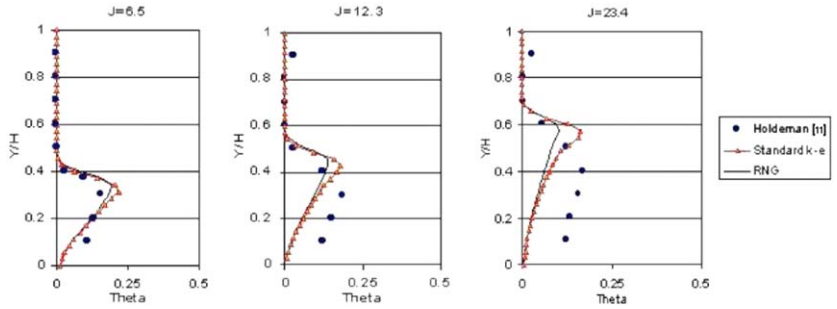

Fig. 7. Influence of momentum flux ratio on the temperature profiles ($S/D = 4$, $H/D = 12$, $X/H = 1$).

k–ε model was more compatible with the experimental results, at various axial positions downstream of jets. But, as illustrated in Fig. 6, by increasing the lateral distance from the center-plane of the jets, the standard k–ε model showed a slightly better agreement with the experimental data. Hence, Both models displayed a reasonable ability for predicting the variations of θ, but this however depended on the axial and the lateral positions.

Fig. 7 shows that both turbulence models were nearly compatible with the experimental results, up to $J = 12.3$. But, beyond this value, the standard k–ε showed somewhat more acceptable trends, which could be due to the turbulent interaction between two adjacent jets, as demonstrated by the outlet cross-section in Fig. 8c. Also, the temperature contours for various momentum flux ratios are presented in Fig. 8.

The effects of geometrical variables, such as the jet spacing-to-diameter ratio, S/D, and the duct height-to-jet diameter ratio, H/D, on the center-plane temperature profiles, are represented by Figs. 9 and 10. For $S/D = 2$ and $H/D = 8$, the standard k–ε model showed a slightly closer trend to the experimental data. This could be due to the presence of the interaction between the two closest adjacent jets, as illustrated by the outlet cross-section in Fig. 10a.

Fig. 11 shows the effect of different geometrical variables on the jet penetration, at a fixed momentum flux ratio of $J = 6$. It can be seen that an increase in D and S, at a fixed H, resulted in a noticeable increase in the jet penetration. This, as displayed in Fig. 10, would eventually result in

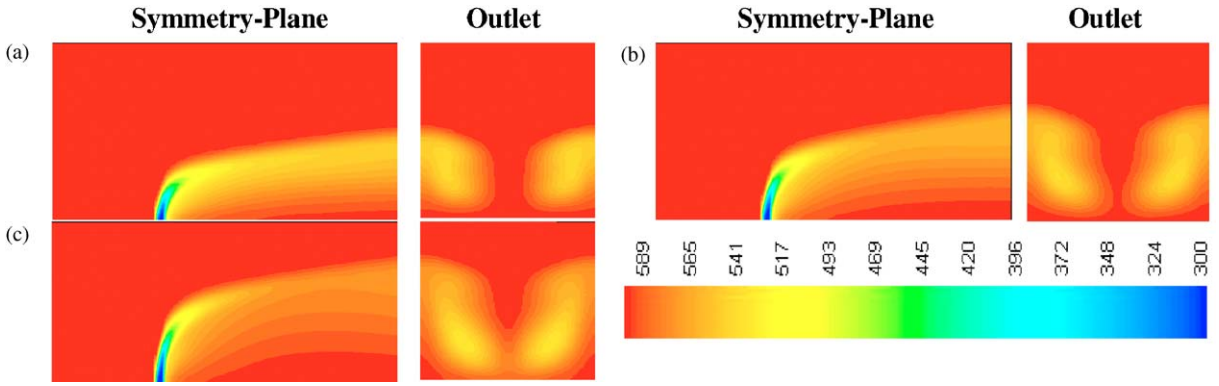

Fig. 8. Temperature contours; (a) $J = 6.5$, (b) $J = 12.3$ and (c) $J = 23.4$.

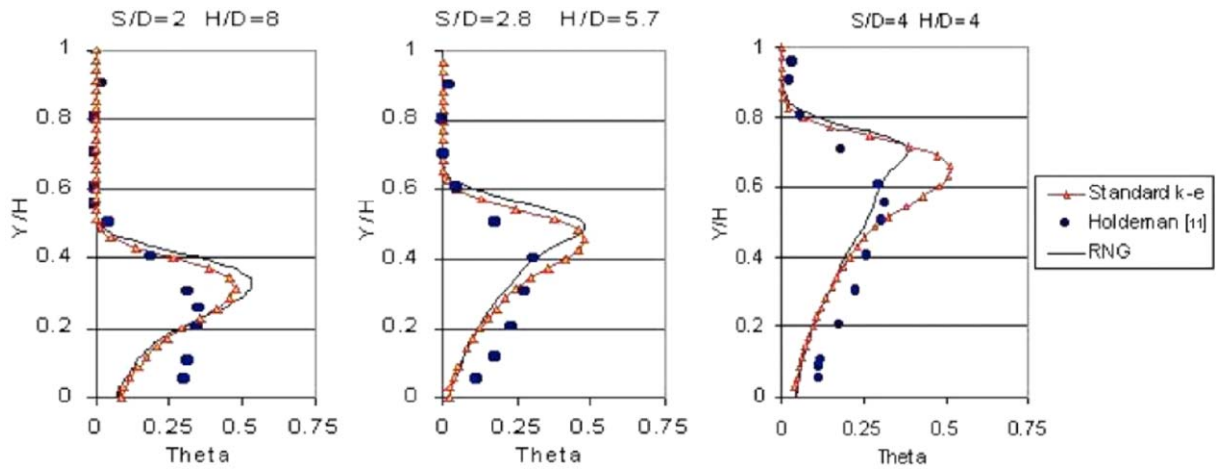

Fig. 9. Effect of geometrical variables on center-plane temperature profiles ($J = 6$, $X/H = 1$, $Z/S = 0$).

the impingement of the jet to the top wall of the duct (Fig. 10c). Hence, at $J = 6$, the optimum geometry was predicted as: $S/D = 2$ and $H/D = 8$. This would prevent the impingement of two opposite jets in the dilution zone of a typical gas turbine combustion chamber, as investigated by Lefebvre [13]. It should be noted that the maximum jet penetration depth must be around $0.4H$ ($Y \approx 0.4H$) [13].

Fig. 12 illustrates the variations of the jet penetration for the optimum geometry, at different values of J. It can be seen that by increasing the momentum flux ratio, the jet penetration was enhanced to values well beyond the maximum (i.e., $Y \approx 0.4H$). Hence, the optimum momentum flux ratio was considered as equal to 6.0.

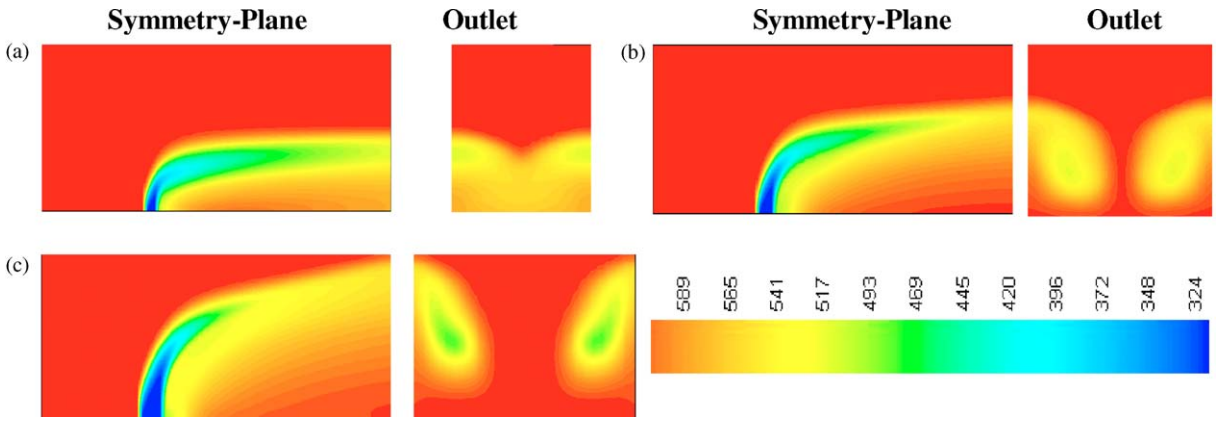

Fig. 10. Temperature contours; (a) $S/D = 2$, $H/D = 8$, (b) $S/D = 2.8$, $H/D = 5.7$ and (c) $S/D = 4$, $H/D = 4$ ($J = 6$).

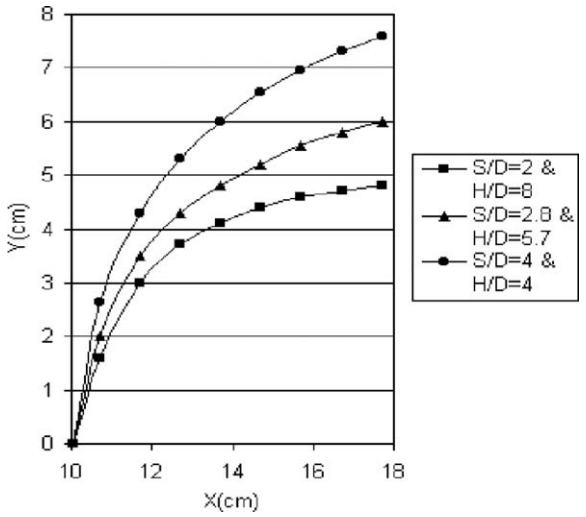

Fig. 11. The jet center-line penetration at $J = 6$, for different geometrical variables.

Fig. 13 demonstrates the velocity vectors for the optimum design condition of $J = 6$, $S/D = 2$ and $H/D = 8$, at various sections of the computational domain. The presently proposed optimum design condition was based on the results of the single-wall injection, which could be extended to conditions encountered in an annular combustion chamber with the opposite-wall injection. Fig. 13a shows the recirculation zone at the cross-section, called the horse-shoe effect [16], which causes a better mixing in the lateral direction. Fig. 13b illustrates the recirculation zone at the downstream section of the injection.

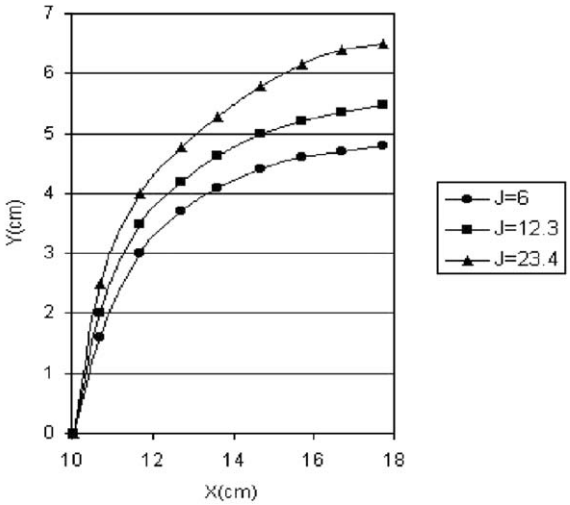

Fig. 12. The jet center-line penetration at $S/D = 2$ and $H/D = 8$, for different momentum flux ratio.

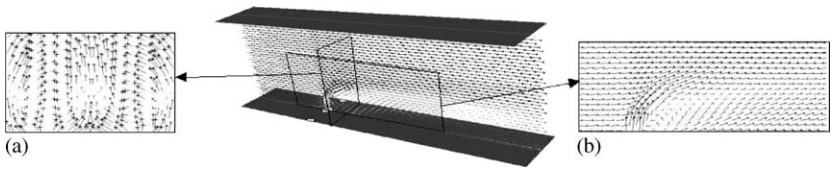

Fig. 13. Velocity vectors for $J = 6$, $S/D = 2$ and $H/D = 8$, (a) Cross-section at $X/H = 0.2$ and (b) Center-plane.

8. Conclusions

A numerical simulation of a non-reacting flow inside a duct was presented for predicting the temperature and flow fields. The following conclusions may be drawn:

(1) Comparisons of the results of two turbulence models with the experimental data of Holdeman and Walker [11] showed that the ability of these models for predicting the temperature profiles, depended on the momentum flux ratio and also on the lateral distance from the centre-line of the jet.
(2) Both turbulence models were nearly compatible with the experimental results, up to $J = 12.3$. But, beyond this value, the standard k–ε showed somewhat more acceptable trends.
(3) An increase in the jet diameter and the jet spacing at a fixed H, resulted in a noticeable increase in the jet penetration.
(4) By increasing the momentum flux ratio, for a fixed geometry, the jet penetration was enhanced.
(5) The optimum design condition, encountered in the dilution zone of an annular combustion chamber, was for the momentum flux ratio of equal to 6 at the geometrical conditions of $S/D = 2$ and $H/D = 8$.

References

[1] F. Bazdidi-Tehrani, A. Haghparast-Kashani, CFD analysis of a single three-dimensional jet injected normally into a crossflow, Proceedings of the Ninth Asian Congress of Fluid Mechanics, May 27–31, 2002, Isfahan, Iran.
[2] F. Bazdidi-Tehrani, A. Shahmir, Turbulent mixing of the single row of coolant jets with a hot confined crossflow: a numerical simulation, Proceedings of the Ninth Asian Congress of Fluid Mechanics, May 27–31, 2002, Isfahan, Iran.
[3] G.B. Cox, An analytical model for predicting exit temperature profile from gas turbine engine annular combustors, AIAA paper (1975) 75–1307.
[4] J.O. Hinz, Turbulence, McGraw-Hill, New York, 1975.
[5] J.D. Holdeman, Mixing of multiple jets with a confined subsonic crossflow, Progr. Energy Combustion Sci. 19 (1993) 31–70.
[6] J.D. Holdeman, D.S. Liscinsky, D.B. Bain, Mixing of multiple jets with a confined subsonic crossflow: part II-opposed rows of orifices in rectangular ducts, J. Engrg. Gas Turbines Power 121 (1999) 551–562.
[7] J.D. Holdeman, D.S. Liscinsky, V.L. Oechsle, G.S. Samuelsen, C.E. Smith, Mixing of multiple jets with a confined subsonic crossflow: part I-cylindrical duct, J. Engrg. Gas Turbines Power 119 (4) (1997) 852–862.
[8] J.D. Holdeman, R. Srinivasan, Modeling dilution jet flow fields, J. Propulsion 2 (1) (1986) 4–10.
[9] J.D. Holdeman, R. Srinivasan, A. Berenfeld, Experiments in dilution jet mixing, AIAA J. 22 (10) (1984) 1436–1443 (also AIAA paper, 83–1201).
[10] J.D. Holdeman, R. Srinivasan, E.B. Coleman, G.D. Meyers, C.D. White, Effects of multiple row and noncircular orifice on dilution jet mixing, J. Propulsion 3 (3) (1987) 219–226.
[11] J.D. Holdeman, R.E. Walker, Mixing of a row of jets with a confined crossflow, AIAA J. 15 (2) (1977) 243–249.
[12] J.T. Kroll, W.A. Sowa, J.S. Samuelsen, J.D. Holdeman, Optimization of orifice geometry for crossflow mixing in a cylindrical duct, J. Propulsion Power 16 (6) (2000) 929–938.
[13] A.H. Lefebvre, Gas Turbine Combustion, 2nd Ed., McGraw-Hill, New York, 1999.
[14] S.V. Patankar, Numerical Heat Transfer and Fluid Flow, Hemisphere Publishing Corporation, Washington, DC, 1980.
[15] S.V. Patankar, D.K. Basu, S.A. Alpay, Prediction of the three-dimentional velocity field of a deflected turbulent jet, Trans. ASME J. Fluids Engrg. 99 (1977) 758–762.
[16] J.W. Ramsey, R.J. Goldstein, Interaction of a heated jet with deflecting stream, Trans. ASME, J. Heat Transfer 94 (1971) 365–372.
[17] H.K. Versteeg, W. Malalasekera, An Introduction to Computational Fluid Dynamics: The Finite Volume Method, 1995, Addison-Wesley Longman, Essex, UK.
[18] D.C. Wilcox, Turbulence Modeling For CFD, DCW Industries, Inc., La Canada, CA, 1993.
[19] S.L.K. Wittig, O.M. Elbahar, B.E. Noll, Temperature profile development in turbulent mixing of coolant jets with a confined hot crossflow, J. Engrg. Gas Turbines Power 106 (193) (1984) 193–197.